Received: 2 September 2019 | Revised: 30 October 2019 | Accepted: 15 November 2019

DOI: 10.1002/prot.25858

RESEARCH ARTICLE

PROTEINS WILEY

Integrative modeling of protein-protein interactions with pyDock for the new docking challenges

Mireia Rosell[1,2] | Luis A. Rodríguez-Lumbreras[1,2] | Miguel Romero-Durana[1,2,3] | Brian Jiménez-García[1] | Lucía Díaz[1] | Juan Fernández-Recio[1,2,3]

[1]Barcelona Supercomputing Center (BSC), Barcelona, Spain

[2]Instituto de Ciencias de la Vid y del Vino (CSIC, Universidad de La Rioja, Gobierno de La Rioja), Logroño, Spain

[3]Structural Biology Unit, Instituto de Biología Molecular de Barcelona (IBMB-CSIC), Barcelona, Spain

Correspondence
Juan Fernández-Recio, ICVV, Ctra. Burgos Km 6, 26007, Logroño, Spain.
Email: juan.fernandezrecio@icvv.es

Present address
Brian Jiménez-García, Bijvoet Center for Biomolecular Research, Faculty of Science—Chemistry, Utrecht University, 3584 CH Utrecht, the Netherlands.

Lucía Díaz, Nostrum Biodiscovery, Jordi Girona 29, 08034 Barcelona, Spain

Funding information
Severo Ochoa program, Grant/Award Number: BIO2016-79930-R; European Union H2020 programme, Grant/Award Number: 676566; SIDRA Medicine; European Regional Development Fund (ERDF) Program Interreg V-A Spain-France-Andorra (POCTEFA); Spanish "Programa Estatal I+D+i"

Peer Review
The peer review history for this article is available at https://publons.com/publon/10.1002/prot.25858.

Abstract

The seventh CAPRI edition imposed new challenges to the modeling of protein-protein complexes, such as multimeric oligomerization, protein-peptide, and protein-oligosaccharide interactions. Many of the proposed targets needed the efficient integration of rigid-body docking, template-based modeling, flexible optimization, multiparametric scoring, and experimental restraints. This was especially relevant for the multimolecular assemblies proposed in the CASP12-CAPRI37 and CASP13-CAPRI46 joint rounds, which were described and evaluated elsewhere. Focusing on the purely CAPRI targets of this edition (rounds 38-45), we have participated in all 17 assessed targets (considering heteromeric and homomeric interfaces in T125 as two separate targets) both as predictors and as scorers, by using integrative modeling based on our docking and scoring approaches: pyDock, IRaPPA, and LightDock. In the protein-protein and protein-peptide targets, we have also participated with our webserver (pyDockWeb). On these 17 CAPRI targets, we submitted acceptable models (or better) within our top 10 models for 10 targets as predictors, 13 targets as scorers, and 4 targets as servers. In summary, our participation in this CAPRI edition confirmed the capabilities of pyDock for the scoring of docking models, increasingly used within the context of integrative modeling of protein interactions and multimeric assemblies.

KEYWORDS
CAPRI, complex structure, multimeric assemblies, protein-oligosaccharide complexes, protein-peptide interactions, protein-protein docking, pyDock

1 | INTRODUCTION

Given the importance of protein-protein interactions in virtually all biomolecular processes, their atomic-level knowledge would be useful for many biomedical and biotechnological applications, such as a better understanding of disease at the molecular level, the interpretation of genomic variants, or the identification of relevant molecules with therapeutic or biotechnological purposes. However, current structural coverage of human interactome is very limited.[1,2] For this reason, computational docking is becoming an essential tool in structural biology, with a growing community of developers providing new methods for the many challenges that the field faces. The center of this is the CAPRI assessment experiment,[3,4] which has been a catalyzer for the docking community, providing new challenges, validation tools, strong consensus on the evaluation of docking performance, and overall, motivating discussions. Over time, the CAPRI experiment has been progressively extended to all varieties of problems related to the structural modeling of protein interactions. As an example of this, the

recent CASP12-CAPRI37[5] and CASP13-CAPRI46[6] joint rounds, which took part during the seventh CAPRI edition, imposed an additional difficulty level in the field of prediction of protein interactions, with a number of multimeric targets in which the docking approaches were fundamental to model many of the oligomeric interfaces. Our performance on the last CASP13-CAPRI round was particularly satisfactory. Considering the CAPRI targets, our group had the third best overall performance of all CASP and CAPRI groups. Regarding CAPRI only groups, we had acceptable models or better within our top five submitted models for 12 targets (out of 20) as predictors (second best group), and for 12 targets (out of 19) as scorers (best group).[6] In most of the cases, the existence of a template to model the assembly was critical. However, in some targets, our pyDock scoring[7] played an important role in the selection of the correct template-based multimeric models among all possible ones. Given that the CASP-CAPRI rounds have been discussed elsewhere,[5,6] we will focus here on the purely CAPRI targets of this edition, which included a number of multimolecular assemblies in addition to the traditional protein-protein binary complexes, together with protein-peptide and challenging protein-saccharide interactions. In all proposed targets, one or more of the components of the complex had no experimental structure and needed to be modeled. In some cases, there were available templates for at least part of the interaction, which encouraged us to integrate template-based modeling, docking, scoring, experimental restraints, and further refinement tools. Overall, this provided a realistic representation of the complexity of the problem of structural modeling of protein interactions. We present here the main aspects of our participation in this CAPRI edition, and the new procedures we devised in response to the challenges proposed by the assessment experiment.

2 | MATERIALS AND METHODS

2.1 | Modeling of subunits with no available structure

In all targets, the structures of one (or more) of the subunits were not available and needed to be modeled before docking. In most of the targets, we used Modeler 9v6 with default parameters[8] based on the template/s suggested by the organizers or on other homologous proteins found by BLAST[9] search tools. The final selected model was the one with the lowest DOPE score.[10] In some cases (eg, T131, T132), highly flexible modeled loops were removed before docking and they were rebuilt in the final models before the minimization phase (see later). In T133, the flexible C-terminal of the ligand was removed and then rebuilt in the final models. In some cases (T121, T123, T124, and T136), we also performed multiple template modeling of any of the interacting subunits with I-TASSER.[11] In the case of the peptides, they were modeled as above described, based on available templates, with some specific considerations that are described in detail for the corresponding targets in the Results section.

2.2 | Generation of docking poses for the predictors experiment

In general, for the protein-protein and protein-peptide targets, we used FTDock[12] (with electrostatics and 0.7 Å grid resolution) and ZDOCK 2.1[13] to generate 10 000 and 2000 rigid-body docking poses, respectively, in the same conditions as previously described,[14] with the exception of a few targets (T131, T132, and T136) in which ZDOCK was not used. For three targets (T131-T133), we used our LightDock[15] method to generate an additional set of flexible docking poses, which included explicit backbone flexibility by using the Anisotropic Network Model (ANM)[16] during the sampling process, and the DFIRE[17] and pyDockLite[15] scoring functions. The number of poses generated by LightDock, which depended on the final step of clustering, was 6093, 6005, and 4977 for targets T131, T132, and T133, respectively. As usual, cofactors, water molecules, and solvent ions were not included in our docking calculations. In the multimolecular assemblies, some of the interfaces were built based on available templates. The use of template-based modeling was especially relevant for the target T136. All the details are described for the corresponding target in the Results section.

2.3 | Scoring of docking poses for both the predictors and the scorers experiment

We scored the docking models generated for protein-protein and protein-peptide targets by the above described methods with our default pyDock protocol,[7] based on energy terms previously optimized for rigid-body docking. The binding energy is basically composed of ASA-based desolvation, Coulombic electrostatics, and van der Waals energy (with a weighting factor of 0.1 to reduce the noise of the scoring function). Electrostatics and van der Waals were limited to −1.0/+1.0 and 1.0 kcal/mol for each interatomic energy value, respectively, in order to avoid excessive penalization from possible clashes derived from the rigid-body approach. For target T133, we also applied our new IRaPPA scoring server[18] to the docking models generated by pyDock server. As previously shown,[18] IRaPPA scoring can significantly improve the predictive performance of pyDock scoring in protein-protein binary complexes. However, we did not use this new scoring scheme for the first targets of this round due to time constraints. When we improved the group organization, we managed to include IRaPPA scoring for T133 as mentioned, but then the next targets were not suitable for IRaPPA: T134-135 were protein-peptide targets for which we had not thoroughly evaluated IRaPPA performance, and T136 was a challenging multimolecular assembly, in which the devised ad hoc modeling strategy made it impractical to include the scoring of binary complexes by IRaPPA. Nevertheless, a retrospective analysis of the use of IRaPPA on the protein-protein targets was performed later, as described in the Conclusions section.

In most of the targets, we were able to define possible interface residues based on experimental information available in the literature (T122, T125, T131, and T132) or from homologous complex

structures (T121, T134, T135, and T136). This information was usually included in the final scoring as distance restraints with pyDockRST.[19] In some cases (T125), we filtered out the docking models incompatible with the estimated position of the membrane. In the case of the peptides, we forced docking models to adopt antiparallel β-strand orientation (which turned out to be correct for targets T134 and T135, but incorrect for target T121). Cofactors, water molecules, and solvent ions were not considered for scoring. After scoring, we eliminated redundant predictions by using a BSAS algorithm[20] with a distance cutoff of 4.0 Å, as previously described.[21] In the case of template-based or symmetry-based models, we eliminated those ones with strong clashes that would be difficult to solve with minimization.

The final 10 selected docking poses were minimized by using different versions of AMBER (AMBER12[22] or AMBER17[23]), with AMBER ff99SB and GAFF force field[24] with implicit solvent in order to improve the quality of the docking models and reduce the number of interatomic clashes, as previously described.[25] The minimization protocol consisted in a 500-cycle steepest descent (SD) minimization with harmonic restraints applied at a force constant of 25 kcal/(mol·Å^2) to all the backbone atoms in order to optimize the side chains, followed by another 500 cycles of conjugate gradient (CG) minimization without restraints. In some cases, due to time constraints or because of earlier convergence, the minimization protocol varied (eg, in T134, we used 200-cycle SD and 300-cycle CG; in T135 500-cycle SD and 100-cycle CG; in T136 some models were not minimized, or were minimized in vacuum). In targets T131 and T132, the loops previously removed for docking were rebuilt by using Modeller before the final minimization step.

The scoring and minimization protocol that we used for the docking models generated as predictors were basically applied in the same way to the set of models provided for scorers (exceptions: no distance restraints as scorers in T121 and T136; IRaPPA was not used as scorers in T133).

2.4 | Docking and scoring for the servers experiment

We participated in all protein-protein and protein-peptide targets with our pyDockWeb server (https://life.bsc.es/servlet/pydock).[26] The generation of docking poses and further scoring were done in a fully automatic manner by FTDock and pyDock, as previously described. In some targets, we used the same interface residue restraints (T122, T131, and T132) or the same membrane-based filtering (T125) as in predictors, but in general, we used much less external data to process the models than in predictors due to time constraints. In multimolecular assemblies, additional modeling steps were performed based on the docking models provided by the server (more details for each target in the Results section). Finally, the best-scored server predictions were clustered and minimized according to our default protocol before submission to CAPRI (with the exception of T122, in which final models were not minimized, and T131 and T132, in which the loops removed before docking were rebuilt by using Modeller with no further minimization).

2.5 | Modeling of protein-saccharide complexes

For the protein-saccharide targets (T126-130), we used rDock[27] (http://rdock.sourceforge.net/) to generate and score the models. Additionally, we developed a new pyDock module specially adapted for the scoring of saccharide molecules. This new module can read topology (*.prmtop*) and coordinate (*.inpcrd*) files from AMBER, using a dictionary of atom types based on AMBER94. This enables loading the data from the oligosaccharide molecule in order to compute the energy-based scoring function. To obtain these files, we first applied *antechamber* to the saccharide molecule with the AM1-BCC charge model,[28] setting the net charge to 0, and then *parmchk2* to obtain a.*frcmod* file with the charges, bond and angular parameters, and a. *mol2* file. Then we used *LEaP* to load the general forcefield of AMBER (GAFF) and followed the procedure to generate a new saccharide library with the information obtained from *antechamber*. As a final step, we used *LEaP* to obtain the coordinates (*.incrd*) and topology (*.prmtop*) files for each protein-saccharide docking pose, in order to be scored with pyDock. The electrostatics energy was calculated as in standard pyDock,[7] using the atom charges obtained as described earlier. The van der Waals energy was calculated with the Lennard-Jones parameters corresponding to the AMBER types of the saccharide atoms. Regarding the desolvation energy term, the saccharide C atoms were assigned the same atomic solvation parameters (ASPs) as "C aliphatic" in pyDock,[7] while the O atoms were assigned the same ASPs as "O hydroxyl" in pyDock.

The center of the cavity used in rDock docking was defined as the center of masses of known ligands bound to homologous proteins (PDB 5F7V for T126-T129; PDB 3D5Z for T130). Thus, we submitted two sets of models. The models 1 to 5 were obtained as scored by rDock, and the models 6 to 10 were obtained as scored by pyDock. For scorers, we used another charge model due to time constraints, the Gasteiger-Marsili empirical atomic partial charges,[29] and the final scoring was only based on this new pyDock version adapted to glucide interactions.

3 | RESULTS AND DISCUSSION

In this CAPRI edition, we participated in all the proposed targets, as predictors, servers, and scorers (with the exception of the protein-saccharide cases, in which our server did not participate since it was not ready for this type of interactions). Our participation in the two CASP-CAPRI joint rounds is described elsewhere.[5,6] Here, we report about our results for the 17 purely CAPRI targets (considering hetero- and homomeric interfaces in T125 as two separate targets), which are summarized in Table 1. When considering our top 10 models, as in past editions, we submitted acceptable models (or better) for 10 targets as predictors, four targets as servers, and 13 targets as scorers. This is a success rate of 59% (predictors), 33% (servers), and 76% (scorers) with respect to the targets in which we participated, which is consistent with our trajectory in CAPRI. The performance as scorers was especially good, actually the best of all participants. If we consider

TABLE 1 Summary of our participation in the seventh CAPRI edition

Target[a]	Type[b]	Predictors[c]	Servers[c]	Scorers[c]
Protein–protein				
T122	$AB_U:C_H$	0	**M08***	**M08** (M05*)**
T123	$A_U:B_H$	0	0	0
T124	$A_U:2B_H$	0	0	0
T125 *hetero*	$2A_U:4B_H$	0/0	0/0	**M02**/0**
T125 *homo*	$2A_U:4B_H$	**M01***/0**	**M01***/0**	**M02*** (M01**)/0**
T131	$A_U:B_H$	0	0	**M06****
T132	$A_H:B_U$	0	0	**M08****
T133	$A_H:B_H$	**M01****	**M05***	**M02****
T136	$10A_H$	**M01**/M02*/M07***	0 [M01**]/0 [M01*]/0	**M02** (M01*)/M02**/M08** (M02*)**
Protein-peptide				
T121	$A_U:Pep_H$	0	0	0
T134	$2A_U:Pep_H$	**M03***	0	**M09****
T135	$2A_U:Pep_H$	**M01***	**M02***	**M01*****
Protein-saccharide				
T126	$A_H:Lig_U$	**M08** (M03*)**	-	**M08***
T127	$A_H:Lig_U$	**M01***	-	0
T128	$A_H:Lig_U$	**M02***	-	**M10** (M01*)**
T129	$A_H:Lig_U$	**M02***	-	**M09** (M02*)**
T130	$A_U:Lig_U$	**M02** (M01*)**	-	**M06****

[a]Underscored: target of special difficulty, with only three or fewer groups that submitted correct models within their top five submitted ones.
[b]Oligomerization type: A, B, and C indicating different subunits, Pep peptide, and Lig oligosaccharide. Subscript indicates the type of available structure for each subunit: U, unbound; H, homology-based model.
[c]Correct models submitted to CAPRI by our group within our top 10 submissions. Each model is numbered according to its rank within our submission. The quality of each model is indicated, following CAPRI criteria: *acceptable; **medium quality; and ***high quality. In bold, our best-quality model for each target. "0": no correct model was submitted. "-": no submissions. Different evaluated interfaces are separated by a slash. In parenthesis, we indicated if there were another successful model within our top 5 or top 1 submissions. For T136, in square brackets, we indicate acceptable or medium-quality models that were disqualified due to clashes.

only our top 5 models, as it is now the consensus in CAPRI in order to be more realistic for practical applications, we submitted acceptable or better models for 10, 3, and 8 targets as predictors, servers, and scorers, respectively. When comparing our performance on the top 5 submitted models with respect to that based on the traditional top 10, the results as predictors and servers did not change too much, but we had a significant drop in performance as scorers. In the following, we will describe in detail the most relevant targets and will try to understand better the rationale behind our performance.

3.1 | Protein-protein targets

3.1.1 | Target T122 (unbound/model)

This target consisted in the human cytokine receptor complex formed by IL-23 (composed of two chains IL-23A and IL-12B) and the receptor IL-23R. The structure of the complex at 2.8 Å resolution is now available, with PDB code 5MZV).[30] The structure of unbound IL-23 was provided (it is now available at 2.5 Å resolution with the PDB code 5MXA),[30] while for IL-23R only the sequence was given. We modeled it based on a homologous template (PDB 1I1R, 25% SI; Table S1), which had three conserved disulfide bonds. We found in the literature that Trp156 in IL-23A was important for the interaction,[31] so we used it as a distance restraint, in the context of our standard docking protocol as servers, predictors, and scorers (see the Methods section). We submitted an acceptable model as servers and a medium model as scorers within our 10 models. If we consider only our best-ranked 5 models, we submitted an acceptable model as scorers (Table 1, Figure 1). However, we did not submit any acceptable model as predictors, although our rank 9 model was not too bad (L-RMSD 13.3 Å). The main difficulty was to identify which of the topologically similar three domains of IL-23R was interacting with IL-23. This was a difficult target for which only 9 predictor groups had acceptable models within the top 5 submitted models. We could speculate that a possible reason for failure is the nanobody needed for the crystallization of the complex, since it was not considered in our modeling. However, it is unlikely that the nanobody is affecting the complex orientation in this case, since it is far

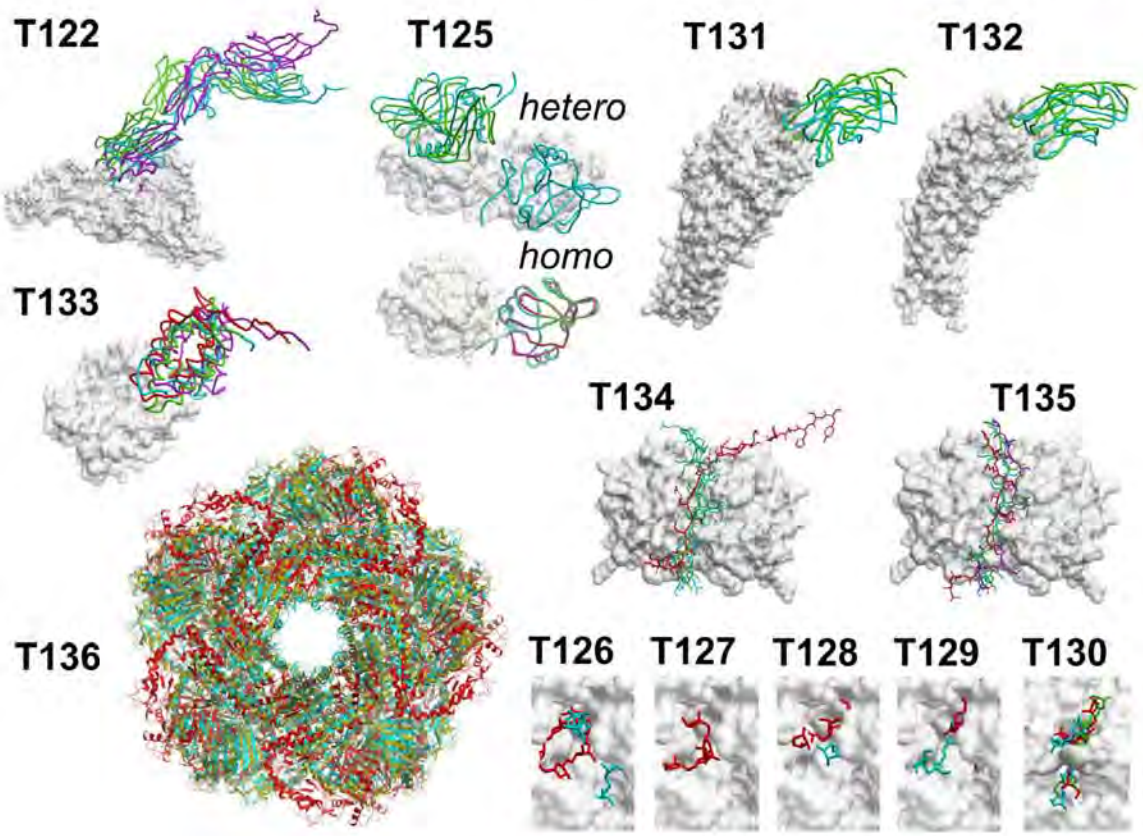

FIGURE 1 Models submitted to CAPRI by our group for successful targets. For each target, receptors are superimposed and shown in white. Ligand in our best model as servers is shown in magenta, as predictors in red, and as scorers in blue. For comparison, the structure of the experimental complex (if available) is represented in green. In T136, we show our model M01 as servers (medium quality but disqualified because of clashes in yellow), our M01 as predictors (in red), and our M02 as scorers (in cyan)

from the interface, and there are other structures in which the molecules show a similar conformation with or without the nanobody (eg, PDB 4GRW, 5MXA). We believe that the major problem in this case is actually related to the difficulties in modeling the IL-23R structure.

3.1.2 | Targets T123, T124 (unbound/model)

These two targets were different complexes related to the same protein. T123 was a complex of a nanobody (nb02) with the N-terminal domain of PorM, while T124 was a complex between another nanobody (nb130) and the dimeric C-terminal domain of PorM. The reference complex structure of the latter is now available (PDB 6EY6).[32] The available structures of the unbound nanobodies (PDB 5LMW and 5FWO, respectively; Table S1) were used in predictors. However, due to incomplete search, in the servers experiment we overlooked these structures and had to model the nanobodies based on homologous templates (PDB 5BOZ, 76% SI for T123; PDB 4GRW, 78% SI for T124). The structures of the monomeric PorM domains were modeled with I-TASSER (Table S1). For the N-terminal domain, we built five models. For the C-terminal domain, only one of the five models built by I-TASSER showed a reasonable structure (the other ones had significantly unstructured regions), and now we checked that even this model had a large structural deviation (RMSD 13 Å) with respect to the conformation in the complex structure (PDB 6EY6). In any case, being unaware of its low quality, we selected this model and tried to increase conformational variability by generating an ANM-based ensemble (20 conformations) using ProDy[33] with default parameters (maximum amplitude 2 Å). From this ensemble, we selected the models with reasonable bond geometry, yielding a total of seven models. The dimeric structure of C-term PorM domain was modeled by superimposing the monomeric models onto the remotely homologous dimeric structure PDB 3MTR (16.7% SI). We applied our standard protocol as servers, predictors, and scorers (see the Methods section). For the assessment, in addition to the heteromeric interfaces, the dimeric interface of the C-term PorM domain was also evaluated. However, we did not submit any acceptable model for these targets (Table 1). They were very challenging for everyone, since there was not a single acceptable model within the top 5 (or even top 10) submitted models among all participants. We could speculate that complexes involving nanobodies are particularly challenging for current docking methods, but the major reason of failure in this case seems to be the difficulties in modeling the PorM domains.

3.1.3 | Target T125 (homodimer unbound/two homodimer models)

This target was a heterohexameric complex formed by an LLT1 homodimer and two NKR-P1 homodimers. The reference complex structure is now available (PDB 5MGT). There were several structures for unbound LLT1 homodimer. We initially used PDB 4WCO as servers, in which there was some missing residues in chain B, so we used Modeller to rebuild them. Then we found a better structure, which we used for predictors (PDB 4QKH).[34] The unbound NKR-P1 homodimer was not available, so it was modeled based on PDB 3T3A (47% SI). As a general strategy, we docked LLT1 homodimer vs NKR-P1 homodimer, and then built the second NKR-P1 by symmetry (this assumption turned out not to be correct, since there are two different LLT1:NKR-P1 interfaces in the complex structure, now available). We removed the docking poses where the ligands overlapped with the estimated position of the membrane.[35] As predictors, we added distance restraints (10 Å interatomic cutoff) derived from residues identified in the literature as potentially involved in the interaction (LLT1 Lys169, and NKR-P1 Glu205).[35,36] This target had four different interfaces (LLT1:NKR-P1/LLT1-LLT1/alternative LLT1:NKR-P1/NKR-P1:NKR-P1), and the heteromeric and homomeric interfaces were independently assessed, as two different targets. We had high-accuracy models for the LLT1-LLT1 interface as servers, predictors, and scorers, which were actually built by standard template-based modeling (Table 1, Figure 1). Interestingly, we identified a medium model for the LLT1:NKR-P1 interface as scorers.

3.1.4 | Targets T131, T132 (unbound/model)

These two targets consisted in two different complexes of hCEACAM1 protein with HopQ type I (T131) and HopQ type II (T132). Reference complex structures are now available with PDB codes 6GBG and 6GBH, respectively.[37] The unbound structure of hCEACAM1 was available (PDB 4WHD),[38] but we used Modeller to build the missing residues at the N-term and C-term. The structures of HopQ type I and HopQ type II were modeled based on a homologous template (PDB 5LP2, SI 96% and 57%, respectively). Before docking, we removed the loops with uncertain conformation (in HopQ type I: 22:28, 113:127, 224:233, 343:351; in HopQ type II: 26:40, 122:125, 229:238, 345:355). We applied our standard protocol for servers. For predictors, we generated docking models with FTDock as well as with LightDock (using pyDockLite and DFIRE as scoring functions), after which all docking poses were rescored by pyDock. For servers and predictors, the missing loops in HopQ type I or II were rebuilt for the best-ranked 100 docking poses before the minimization step, thus providing implicit flexibility to the docking procedure. For this, from all the full-length models generated by Modeller for each docking pose, we selected the best five ones according to DOPE score, and from them, we took the one with fewer atomic clashes between the built loops and hCEACAM1. As scorers, we followed our standard pyDock protocol (but we did not rebuild the docking poses provided in the scorer set). In all cases (as servers, predictors or scorers), distance restraints were imposed based on two potential interface residues in hCEACAM1 (Tyr35 and Ile92).[39] We did not submit any acceptable model within our best-ranked five models, either as servers, predictors, or scorers, but we had medium models as scorers for both targets within our top 10 models (Table 1, Figure 1). These were challenging targets, with only 1 and 3 predictor groups, and 4 and 6 scorers, respectively, submitting acceptable models within the top 10 models.

3.1.5 | Target T133 (model/model)

This target consisted in a redesigned complex between colicin E2 DNAse and Im2. The reference complex structure is now available (PDB 6ERE).[40] None of the unbound structures for the redesigned proteins was available, but the original complex with the unmodified sequence was a past CAPRI target (T47) and its structure was available with PDB code 3U43.[41] Thus, we modeled E2 DNAse based on chain B (87% SI) and Im2 on chain A (83% SI), removing its C-terminal part because of its expected high flexibility (Table S1). We applied our standard protocol for servers. For predictors, we submitted two sets of interactions. The first 5 models were obtained from docking poses generated by FTDock and rescored by IRaPPA. The models 5-10 came from docking poses generated by FTDock, ZDOCK, and LightDock (with pyDockLite and DFIRE functions) and rescored by pyDock. For scorers, we applied our standard pyDock protocol. Within our top 5 submitted models, there were acceptable models (as servers) and medium ones (as predictors and scorers) (Table 1, Figure 1). Interestingly, the medium model submitted as rank 1 for predictors was obtained with the new IRaPPA scoring.

3.1.6 | Target T136 (homodecamer model)

This target consisted in the EM structure of the bacterial LdcA complex, forming a homodecamer with D5 symmetry. The structure of the unbound monomer was not available, so we modeled it based on PDB 5FKZ chain E (45% SI). For the overall complex arrangement, there were available templates (PDB 2VYC, with 40% SI, is an X-ray structure at 2.4 Å resolution; PDB 5FKZ, with 45% SI, is an EM structure at 5.5 Å resolution; Table S1). For servers, our two first submitted models were built directly superimposing the monomer model on the available templates. The rest of the models were generated by docking the monomer models with the standard FTDock + pyDock protocol, with distance restraints derived from the estimated interface residues from the 5FKZ template (using 10 Å distance cutoff), and superimposing the binary docking models on the global template (PDB 5FKZ). As predictors, we had a more elaborated strategy. Four models were built by superimposing two different monomer models (by Modeller and I-TASSER) on the two different decamer templates (PDB 2VYC and

5FKZ). Then another 102 models were built by using the two decamer models based on 5FKZ as templates for global modeling with Modeller, building for each of them 1 model, plus additional 50 models with symmetry restraints. Another 20 000 models were built by docking each of the monomer models with FTDock, using distance restraints on each docking dimer model based on the interface residues of the templates, and superimposing each binary docking pose on the decamer template as in servers. Finally, a set of 6 models were built from the previously generated docking dimer models that were closer in RMSD to the interface involving the N-terminal wing domain in both templates.[42] All the models were merged in a single pool and sorted according to pyDock scoring. For scorers, we applied the standard pyDock scoring to all interfaces of each decamer decoy, being the final score the sum of that of each interface, with no other additional restraint. This target had three different monomer-monomer interfaces, which were individually assessed. Our best submission for servers had medium and acceptable quality for the first and second interfaces, but it was disqualified due to clashes. As predictors and scorers, we had acceptable or medium models for all the interfaces (Table 1, Figure 1), in most of the cases from our best or second best submission. As predictors, our two best-ranked models followed this integrative template-based modeling strategy: pyDock scoring of the refined decamer models generated with Modeller based on the initial decamers built by superimposing the monomer models on the decamer template PDB 5FKZ.

3.2 | Protein-peptide targets

3.2.1 | Target T121 (unbound/peptide model)

This target consisted in the interaction between TolA and a 13-residue fragment of TolB. The structure of unbound TolA was available (PDB 1LR0), but for TolB fragment only the sequence was provided. Five models for TolB fragment were built with I-TASSER, and independently docked to TolA structure as servers, following our standard pyDockWeb protocol. For predictors, we applied Modeller to built 20 models of TolB fragment using PDB 2HQS as a template, and another 20 models using PDB 2W8B as a template (Table S1). We docked all of these 40 models independently to TolA, using FTDock and ZDOCK, and imposing distance restraints based on PDB 1TOL (a fusion protein formed by a TolA domain and a g3p domain with potentially similar β-strand interaction). We applied our standard pyDock scoring protocol either as predictors or as scorers. In all cases, as servers, predictors, or scorers, only docking decoys with antiparallel β-strand orientation were selected, which turned out to be a wrong decision according to the data presented and discussed during the seventh CAPRI evaluation meeting in Hinxton (UK). As a consequence, no acceptable models were found in any of our submissions (Table 1). In any case, this was a difficult target, with only three predictor groups with acceptable models within the top five submissions.

3.2.2 | Targets T134, T135 (unbound/peptide model)

These targets were based on the interaction between the DLC8 dimer and a 12-residue myelin-associated glycoprotein fragment. The reference complex structure is now available (PDB 6GZL).[43] The NMR structure of the unbound DLC8 dimer was available (PDB 1F3C),[44] but the structure of the peptide was not. Moreover, for the first target (T134), not even the sequence of the peptide was provided. The goal was to identify the 12-residue peptide sequence within the 57-residue segment of P20917. For this, we used T-COFFEE[45] and Clustal Omega[46] to align the 57-residue target sequence with available templates (PDB 1F95, 1F96, and 3P8M; the latter identified with DOCKGROUND[47]). Thus, for servers we used Modeller to build models from templates 1F96 and 3P8M using Clustal Omega alignments, selecting those with β-sheet conformation with special focus on SXSXSX sequence motif, which resulted in one model from 1F96 aligned in RGESPELDLSYSHSD, two models from 3P8M aligned in SYSHSDLGKRP, and another one aligned in LGSERRL. For predictors, we built more models, using additional alignment strategies as follows. From 1F95 template, we used Clustal Omega and T-COFFEE to obtain DLSYSHSDLGK and RPTKDSYTLTE fragments (the latter turning out to be the correct one), from 1F96 using Clustal Omega and T-COFFEE we obtained ESEKRLGSERR fragment, and from 3P8M with T-COFFEE we obtained ESEKRLGSERR fragment. For each of these fragments, 20 models were built with Modeller, and those with β-sheet conformation were selected, which resulted in 10 models. Additionally, we used SCWRL[48] to model the residue side chains in the four template fragments described earlier, which resulted in another four more models.

We docked these models to the first NMR structure of DLC8 dimer (PDB 1F3C) following our standard pyDock protocol for servers and predictors (see the Methods section). In all cases (servers, predictors, and scorers), only docking decoys with β-strand antiparallel orientation were selected (which this time turned out to be a correct decision), and distance restraints were imposed, derived from the two binding sites of DLC8 dimer with another peptide in PDB 1F95. Binding residues at 5 Å from the peptide were used as distance restraints for docking (we should note that we did not use this complex structure for template-based modeling; we submitted only models derived from docking). Since a DLC8 dimer could have two symmetric peptide binding sites (one for each monomer), we checked carefully the fulfillment of restraints not only for the ligand bound in each docking model but also for the symmetric ligand position in the other DLC8 monomer. We performed clustering (2 Å ligand RMSD cutoff), clash removal, and minimization following our standard protocol (see the Methods section). For scorers, we applied pyDock scoring, using the same distance restraints, β-strand orientation selection, clustering, clash removal, and minimization steps as in predictors.

For the second target (T135), the 12-residue sequence was provided. Seven models of this peptide were built based on the two models submitted as predictors for T134 that matched the sequence, as well as on our best-ranked five models submitted as scorers for

T134. We docked all these models to the 20 NMR models of DLC8 (PDB 1F3C). The scoring of the protein-peptide models as servers, predictors, or scorers was based on pyDock, using the same distance restraints, β-strand orientation selection, clustering, clash removal, and minimization steps as in T134.

For T134, we obtained an acceptable model as predictors within our top 5 submitted models, and a medium model as scorers within the top 10 submitted models. For T135, we obtained acceptable models for servers and predictors (model ranked second and first, respectively), and a high accuracy model as our rank-1 submission (Table 1, Figure 1). This confirms the excellent capabilities of pyDock for the scoring of docking decoys, regarding not only protein-protein complexes but also protein-peptide ones.

3.3 | Protein-saccharide targets

3.3.1 | Targets T126-T130 (model, unbound/arabino-oligosaccharide model)

Targets T126-T129 consisted in different complexes of arabino-oligosaccharide binding protein (AbnE) with arabino-oligosaccharides of different lengths: arabinotriose (A3), arabinotetraose (A4), arabinopentaose (A5), and arabinohexaose (A6), respectively. None of these targets have their complex structure released yet. Target T130 was a complex of arabinanase (AbnB) with arabinopentaose (A5), and its reference structure is now available (PDB 6F1G).[49] The structure of AbnE was modeled based on a homologous template with PDB 5F7V (30% SI). The structure of the unbound AbnB mutant was available (PDB 3D5Z). We used SCWRL to mutate Gly9 residue to Asn as in WT, and kept water molecules 501 and 658, which were found to be important for the catalytic activity.[50] Regarding the structure of the arabino-oligosaccharides, we used Maestro[51] (Schrödinger) to build six models for A3 based on PDB 2C7F, 2X8S, and 3QEF, as well as on PubChem CID 53356682; one model for A4 based on PubChem CID 74539968; three models for A5 based on PDB 5HOF and PubChem CID 74539969; and four models for A6 based on PDB 1GYE and PubChem CID 74539970. All ligands from PDB files were prepared with *ligprep* for the docking. We did not participate as servers, since pyDockWeb cannot automatically deal with this type of interactions. To generate the docking models in predictors, we used rDock (see the Methods section). Based on the ligands bound to a homologue of AbnE (PDB 5F7V) and the x-ray structure of AbnB (PDB 3D5Z), we defined the center of the cavity for the docking calculations. Our models ranked 1 to 5 (M01-05) were selected according to rDock scoring, while models 6 to 10 (M06-10) were selected after scoring by an updated version of pyDock with parameters adapted for saccharides. As scorers, the protein-saccharide models were all selected according to this new pyDock version alone. We obtained acceptable or medium models within our top 10 submissions in all cases as predictors or scorers, except in T127 as scorers (Table 1, Figure 1). Regarding our top 5 submissions (M01-05), in the case of predictors these models came from rDock scoring as explained earlier, and produced acceptable models in all five cases (one of them was medium accuracy). In the case of scorers, the models were selected by pyDock scoring as mentioned earlier, which produced acceptable models in only two cases. The performance of pyDock scoring in scorers showed slightly worse ranking capabilities than rDock in predictors.

4 | CONCLUSIONS

With this seventh CAPRI edition, we have continued our active involvement in CAPRI activities. The two CASP-CAPRI rounds in this CAPRI edition imposed new challenges for our docking and scoring approaches, which were integrated in a broader modeling scheme, including docking, template-based modeling, flexible refinement, and experimental restraints. The scoring function from pyDock was particularly successful for the multimeric targets of the last CASP13 edition. For the purely CAPRI rounds, we have submitted models for all targets as predictors and scorers, and our server pyDockWeb has participated in all protein-protein and protein-peptide targets. Our scoring scheme pyDock has been used to rank models generated by different approaches (mostly FTDock, ZDOCK, and occasionally LightDock or homology-based models). As predictors, we failed in the most difficult targets, but succeeded in the majority of the remaining ones. Interestingly, the use of IRaPPA scoring in T133 was the reason of the successful predictions. However, when we retrospectively applied this scoring scheme to the rest of protein-protein targets for which standard pyDock scoring did not work well as predictors (T122-125 and T131-132; excluding T136, a challenging multimolecular assembly, in which the devised ad hoc modeling strategy made it impractical to include IRaPPA scoring of binary complexes), we would have obtained successful predictions within top 10 models only in one target (T131). In most of the other targets, the main problem was the poor quality of the models built for one or both interacting subunits, which IRaPPA scoring cannot help to overcome. The performance as servers for the protein-protein and protein-peptide targets was only slightly worse than that as predictors. As scorers, we had excellent performance when considering top 10 submitted models (best of all participants). However, the results were slightly worse when considering top 5 models. This could be due to the fact that pyDock scoring was optimized in the past for the scoring of rigid-body docking poses, and perhaps it is not fine-tuned for the increasingly refined protein-protein docking models generated by the community. As usual, our participation in CAPRI and the analysis of our results and those of the other groups is an excellent source of inspiration for our next developments in the protein-protein docking field.

ACKNOWLEDGEMENTS

This work has been funded by grant number BIO2016-79930-R from the Spanish "Programa Estatal I+D+i", "PIREPRED" grant from the EU European Regional Development Fund (ERDF) Program Interreg V-A Spain-France-Andorra (POCTEFA), Research Contract with SIDRA Medicine (Qatar), and contract 676566 (grant "MuG") from the European Union H2020 programme. B. J. -G. and M. R. were supported by FPI fellowships from the Spanish "Programa Estatal I+D +i" and the Severo Ochoa program, respectively.

ORCID

Lucia Díaz https://orcid.org/0000-0001-8850-2571

Juan Fernández-Recio https://orcid.org/0000-0002-3986-7686

REFERENCES

1. Venkatesan K, Rual JF, Vazquez A, et al. An empirical framework for binary interactome mapping. *Nat Methods*. 2009;6(1):83-90.
2. Stumpf MP, Thorne T, de Silva E, et al. Estimating the size of the human interactome. *Proc Natl Acad Sci U S A*. 2008;105(19):6959-6964.
3. Méndez R, Leplae R, De Maria L, Wodak SJ. Assessment of blind predictions of protein–protein interactions: current status of docking methods. *Proteins*. 2003;52(1):51-67.
4. Lensink MF, Méndez R, Wodak SJ. Docking and scoring protein complexes: CAPRI 3rd edition. *Proteins*. 2007;69(4):704-718.
5. Lensink MF, Velankar S, Baek M, Heo L, Seok C, Wodak SJ. The challenge of modeling protein assemblies: the CASP12-CAPRI experiment. *Proteins*. 2018;86(S1):257-273.
6. Lensink MF, Brysbaert G, Nadzirin N, et al. Blind prediction of homo- and hetero- protein complexes: the CASP13-CAPRI experiment. *Proteins*. 2019.
7. Cheng TM-K, Blundell TL, Fernandez-Recio J. pyDock: electrostatics and desolvation for effective scoring of rigid-body protein–protein docking. *Proteins*. 2007;68(2):503-515.
8. Sali A, Blundell TL. Comparative protein modelling by satisfaction of spatial restraints. *J Mol Biol*. 1993;234(3):779-815.
9. Altschul SF, Gish W, Miller W, Myers EW, Lipman DJ. Basic local alignment search tool. *J Mol Biol*. 1990;215(3):403-410.
10. Shen MY, Sali A. Statistical potential for assessment and prediction of protein structures. *Protein Sci*. 2006;15(11):2507-2524.
11. Roy A, Kucukural A, Zhang Y. I-TASSER: a unified platform for automated protein structure and function prediction. *Nat Protoc*. 2010;5:725.
12. Gabb HA, Jackson RM, Sternberg MJ. Modelling protein docking using shape complementarity, electrostatics and biochemical information. *J Mol Biol*. 1997;272(1):106-120.
13. Chen R, Weng Z. A novel shape complementarity scoring function for protein-protein docking. *Proteins*. 2003;51(3):397-408.
14. Grosdidier S, Pons C, Solernou A, Fernandez-Recio J. Prediction and scoring of docking poses with pyDock. *Proteins*. 2007;69(4):852-858.
15. Jiménez-García B, Roel-Touris J, Romero-Durana M, Vidal M, Jiménez-González D, Fernández-Recio J. LightDock: a new multi-scale approach to protein–protein docking. *Bioinformatics*. 2017;34(1):49-55.
16. Doruker P, Atilgan AR, Bahar I. Dynamics of proteins predicted by molecular dynamics simulations and analytical approaches: application to alpha-amylase inhibitor. *Proteins*. 2000;40(3):512-524.
17. Liu S, Zhang C, Zhou H, Zhou Y. A physical reference state unifies the structure-derived potential of mean force for protein folding and binding. *Proteins*. 2004;56(1):93-101.
18. Moal IH, Barradas-Bautista D, Jiménez-García B, et al. IRaPPA: information retrieval based integration of biophysical models for protein assembly selection. *Bioinformatics*. 2017;33(12):1806-1813.
19. Chelliah V, Blundell TL, Fernandez-Recio J. Efficient restraints for protein-protein docking by comparison of observed amino acid substitution patterns with those predicted from local environment. *J Mol Biol*. 2006;357(5):1669-1682.
20. Theodoridis SK. *Konstantinos. Pattern Recognition*. London (England): Academic Press; 1999.
21. Pons C, Solernou A, Perez-Cano L, Grosdidier S, Fernandez-Recio J. Optimization of pyDock for the new CAPRI challenges: docking of homology-based models, domain-domain assembly and protein-RNA binding. *Proteins*. 2010;78(15):3182-3188.
22. Case D, Darden T, Cheatham III T, et al. AMBER 12; University of California: San Francisco, 2012. There is no corresponding record for this reference. 2010:1–826.
23. Case D, Cerutti DS, Cheatham T, et al. Amber 2017, University of California, San Francisco, 2017.
24. Cheatham TE 3rd, Cieplak P, Kollman PA. A modified version of the Cornell et al. force field with improved sugar pucker phases and helical repeat. *J Biomol Struct Dyn*. 1999;16(4):845-862.
25. Pallara C, Jimenez-Garcia B, Perez-Cano L, et al. Expanding the frontiers of protein-protein modeling: from docking and scoring to binding affinity predictions and other challenges. *Proteins*. 2013;81(12):2192-2200.
26. Jimenez-Garcia B, Pons C, Fernandez-Recio J. pyDockWEB: a web server for rigid-body protein-protein docking using electrostatics and desolvation scoring. *Bioinformatics*. 2013;29(13):1698-1699.
27. Ruiz-Carmona S, Alvarez-Garcia D, Foloppe N, et al. rDock: a fast, versatile and open source program for docking ligands to proteins and nucleic acids. *PLoS Comput Biol*. 2014;10(4):e1003571-e1003571.
28. Jakalian A, Jack DB, Bayly CI. Fast, efficient generation of high-quality atomic charges. AM1-BCC model: II. Parameterization and validation. *J Comput Chem*. 2002;23(16):1623-1641.
29. Gasteiger J, Marsili M. A new model for calculating atomic charges in molecules. *Tetrahedron Lett*. 1978;19(34):3181-3184.
30. Bloch Y, Bouchareychas L, Merceron R, et al. Structural activation of pro-inflammatory human cytokine IL-23 by cognate IL-23 receptor enables recruitment of the shared receptor IL-12Rb1. *Immunity*. 2018;48(1):45-58.e46.
31. Desmet J, Verstraete K, Bloch Y, et al. Structural basis of IL-23 antagonism by an Alphabody protein scaffold. *Nat Commun*. 2014;5:5237.
32. Leone P, Roche J, Vincent MS, et al. Type IX secretion system PorM and gliding machinery GldM form arches spanning the periplasmic space. *Nat Commun*. 2018;9(1):429.
33. Bakan A, Meireles LM, Bahar I. ProDy: protein dynamics inferred from theory and experiments. *Bioinformatics*. 2011;27(11):1575-1577.
34. Skálová T, Bláha J, Harlos K, et al. Four crystal structures of human LLT1, a ligand of human NKR-P1, in varied glycosylation and oligomerization states. *Acta Crystallogr D Biol Crystallogr*. 2015;71(Pt 3):578-591.
35. Kita S, Matsubara H, Kasai Y, et al. Crystal structure of extracellular domain of human lectin-like transcript 1 (LLT1), the ligand for natural killer receptor-P1A. *Eur J Immunol*. 2015;45(6):1605-1613.
36. Kamishikiryo J, Fukuhara H, Okabe Y, Kuroki K, Maenaka K. Molecular basis for LLT1 protein recognition by human CD161 protein (NKRP1A/KLRB1). *J Biol Chem*. 2011;286(27):23823-23830.
37. Moonens K, Hamway Y, Neddermann M, et al. Helicobacter pylori adhesin HopQ disrupts trans dimerization in human CEACAMs. *EMBO J*. 2018;37(13):e98665.
38. Kirouac KN, Prive, G.G. Human CEACAM1 N-domain homodimer. (to be published).
39. Javaheri A, Kruse T, Moonens K, et al. Helicobacter pylori adhesin HopQ engages in a virulence-enhancing interaction with human CEACAMs. *Nat Microbiol*. 2016;2:16189.
40. Netzer R, Listov D, Lipsh R, et al. Ultrahigh specificity in a network of computationally designed protein-interaction pairs. *Nat Commun*. 2018;9(1):5286.
41. Wojdyla JA, Fleishman SJ, Baker D, Kleanthous C. Structure of the ultra-high-affinity Colicin E2 DNase–Im2 complex. *J Mol Biol*. 2012;417(1):79-94.
42. Kandiah E, Carriel D, Perard J, et al. Structural insights into the *Escherichia coli* lysine decarboxylases and molecular determinants of interaction with the AAA+ ATPase RavA. *Sci Rep*. 2016;6:24601-24601.
43. Myllykoski M, Eichel MA, Jung RB, Kelm S, Werner HB, Kursula P. High-affinity heterotetramer formation between the large myelin-associated glycoprotein and the dynein light chain DYNLL1. *J Neurochem*. 2018;147(6):764-783.

44. Fan J-S, Zhang Q, Tochio H, Li M, Zhang M. Structural basis of diverse sequence-dependent target recognition by the 8 kDa dynein light chain11Edited by P. E. Wright. *J Mol Biol*. 2001;306(1):97-108.
45. Di Tommaso P, Moretti S, Xenarios I, et al. T-Coffee: a web server for the multiple sequence alignment of protein and RNA sequences using structural information and homology extension. *Nucleic Acids Res*. 2011;39:W13-W17.
46. Sievers F, Higgins DG. Clustal Omega. *Curr Protoc Bioinformatics*. 2014;48(1):3.13.11-13.13.16.
47. Kundrotas PJ, Anishchenko I, Dauzhenka T, et al. Dockground: a comprehensive data resource for modeling of protein complexes. *Protein Sci*. 2018;27(1):172-181.
48. Canutescu AA, Shelenkov AA, Dunbrack RL Jr. A graph-theory algorithm for rapid protein side-chain prediction. *Protein Sci*. 2003;12(9):2001-2014.
49. Lansky S, Shwartshtien O, Salama R, Shoham Y, Shoham G. The structure of AbnB-E201A, an intracellular 1,5-alpha-L-arabinanase from *Geobacillus stearothermophilus*, in complex with arabinopentaose. http://www.rcsb.org/structure/6F1G; (to be published).
50. Alhassid A, Ben-David A, Tabachnikov O, et al. Crystal structure of an inverting GH 43 1,5-α-L-arabinanase from Geobacillus stearothermophilus complexed with its substrate. *Biochem J*. 2009;422(1):73-82.
51. Schrödinger Release 2019–3: LigPrep, Schrödinger, LLC, New York, NY. 2019.

SUPPORTING INFORMATION

Additional supporting information may be found online in the Supporting Information section at the end of this article.

How to cite this article: Rosell M, Rodríguez-Lumbreras LA, Romero-Durana M, Jiménez-García B, Díaz L, Fernández-Recio J. Integrative modeling of protein-protein interactions with pyDock for the new docking challenges. *Proteins*. 2019;1–10. https://doi.org/10.1002/prot.25858